ROYAL SOCIETY
OF CHEMISTRY

PAPER

Check for updates

The effect of MnCO₃ on the gain coefficient for the ⁴I₁₃/₂ → ⁴I₁₅/₂ transition of Er³⁺ ions and near-infrared emission bandwidth flatness of Er³⁺/Tm³⁺/Yb³⁺ co-doped barium zinc silicate glasses†

Ho Kim Dan, [ID] *[ab] Nguyen Dinh Trung,[cd] Nguyen Minh Tam, [ID] [e] L. T. Ha, [ID] *[f] Nguyen Le Thai,[g] Tran Dang Thanh,[h] Dacheng Zhou[i] and Jianbei Qiu[i]

The roles of Mn²⁺ ions in the MnCO₃ compound, leading to the formation of an Mn²⁺–Yb³⁺ dimer and affecting the gain coefficient for the ⁴I₁₃/₂ → ⁴I₁₅/₂ transition of Er³⁺ ions and near-infrared (NIR) emission bandwidth flatness of Er³⁺/Tm³⁺/Yb³⁺ co-doped in SiO₂–ZnO–BaO (SZB) barium zinc silicate glasses, were investigated in this work. The composition of all elements from the original raw materials that exist in the host glasses was determined using energy-dispersive X-ray spectroscopy (EDS). Under the excitation of a 980 nm laser diode (LD), the NIR emission of Er³⁺/Tm³⁺/Yb³⁺-co-doped SZB glasses produced a bandwidth of about 430 nm covering the O, E, and C bands. The effects of Mn²⁺ ions and the Mn²⁺–Yb³⁺ dimer on the gain coefficient for the ⁴I₁₃/₂ → ⁴I₁₅/₂ transition of Er³⁺ ions and bandwidth flatness of NIR emission of Er³⁺/Tm³⁺-co-doped and Er³⁺/Tm³⁺/Yb³⁺-co-doped SZB glasses were also assigned. The optimal molar concentration of Mn²⁺ ions was determined such that the NIR bandwidth flatness of Er³⁺/Tm³⁺/Yb³⁺-co-doped SZB glasses was the flattest. In addition, the role of Mn²⁺ ions in reducing the gain coefficient for the ⁴I₁₃/₂ → ⁴I₁₅/₂ transition of Er³⁺ ions was also calculated and discussed.

1. Introduction

The near-infrared (NIR) emission spectra of rare earth ions (REIs), such as Pr³⁺, Er³⁺, Tm³⁺, and Ho³⁺ ions, in the wavelength range from ∼1200 to 2000 nm with the coverage of long-band (L-band), ultra-band (U-band), and (L + U)-bands have been of interest to researchers due to their expected applications in optical amplifiers and fibre lasers.[1–3] The NIR emission spectra of the Er³⁺-doped peak at about 1545 nm and of the Tm³⁺-doped peak at about 1769 nm, corresponding to ⁴I₁₃/₂ → ⁴I₁₅/₂ (ref. 4) and ³F₄ → ³H₆ transitions, respectively, have been widely investigated because of their typical applications in an erbium-doped fiber amplifier (EDFA)[5,6] and a thulium-doped fiber amplifier (TDFA).[7] While Er³⁺ ions can be directly excited by commercial wavelengths of both 808 nm LD and 980 nm LD,[1,5,6,8] Tm³⁺ ions can only be directly excited by the wavelength of an 808 nm LD but not by a 980 nm LD.[9,10] Therefore, for the NIR emission spectra of Tm³⁺-doped and Er³⁺/Tm³⁺-co-doped glasses using a commercial wavelength 980 nm LD for excitation, Yb³⁺ ions are often introduced as a sensitizer or for a cooperative energy transfer (CET) process through dimers/trimers such as a Yb³⁺–Yb³⁺ dimer,[11] Cr³⁺–Yb³⁺ dimer,[12] Mn²⁺–Yb³⁺ dimer,[13,14] or Mn²⁺–Mn²⁺–Yb³⁺ trimer[4,15] for direct excitation by the commercial wavelength of a 980 nm LD.[16] Among the dimers, the Mn²⁺–Yb³⁺ dimer formed by transition metal ions Mn²⁺ and Yb³⁺ ions is commonly used for the CET process of NIR emission spectra of Tm³⁺ doped or Er³⁺/Tm³⁺ co-doped in host glasses.[13,14,17] In addition to expanding the NIR spectral bandwidth for REIs, recent studies have also focused on investigating and finding solutions to flatten the NIR spectral bandwidth of these REIs to optimize the obtained NIR spectral bandwidth for optical applications.[18–22] In our previous studies,[23,24] we investigated, calculated, and reported solutions to widen the bandwidth as well as to enhance the near-infrared bandwidth flatness of Tm³⁺-doped, Ho³⁺-doped, Tm³⁺/Ho³⁺-co-

[a]*Optical Materials Research Group, Science and Technology Advanced Institute, Van Lang University, Ho Chi Minh City, Vietnam. E-mail: hokimdan@vlu.edu.vn*

[b]*Faculty of Applied Technology, School of Technology, Van Lang University, Ho Chi Minh City, Vietnam*

[c]*Center for Analysis and Testing, Dalat University, Lam Dong, Vietnam*

[d]*Faculty of Chemistry and Environment, Dalat University, Lam Dong, Vietnam*

[e]*Faculty of Basic Sciences, University of Phan Thiet, 225 Nguyen Thong, Phan Thiet City, Binh Thuan, Vietnam*

[f]*Institute of Science and Technology, TNU-University of Sciences, Thai Nguyen, 250000, Vietnam. E-mail: halt@tnus.edu.vn*

[g]*Faculty of Engineering and Technology, Nguyen Tat Thanh University, Ho Chi Minh City, Vietnam*

[h]*Institute of Materials Science, Vietnam Academy of Science and Technology (VAST), 18 Hoang Quoc Viet, Hanoi, Vietnam*

[i]*Key Laboratory of Advanced Materials of Yunnan Province, Kunming University of Science and Technology, Kunming, 650093, China*

† Electronic supplementary information (ESI) available. See DOI: https://doi.org/10.1039/d3ra06348h

doped, and $Ho^{3+}/Tm^{3+}/Yb^{3+}$-co-doped glasses.[19,23] The obtained results indicated that the NIR bandwidth flatness of Tm^{3+}-doped, Ho^{3+}-doped, Tm^{3+}/Ho^{3+}-co-doped, and $Ho^{3+}/Tm^{3+}/Yb^{3+}$co-doped glasses was significantly improved by the presence of Mn^{2+} ions and an Mn^{2+}–Yb^{3+} dimer in the host glasses.[13,14,23]

Following the positive results described above, in this work, we continue to examine and report the effects of Mn^{2+} ions and Mn^{2+}–Yb^{3+} dimers on the gain coefficient for the $^4I_{13/2} \rightarrow \,^4I_{15/2}$ transition of Er^{3+} ions and NIR emission bandwidth flatness of $Er^{3+}/Tm^{3+}/Yb^{3+}$-co-doped barium zinc silicate glasses with the aim of clarifying the roles of Mn^{2+} ions in the $MnCO_3$ compound in the formation of an Mn^{2+}–Yb^{3+} dimer. Remarkably, we have attempted to determine not only the optimal BFN_NIR emission of $Er^{3+}/Tm^{3+}/Yb^{3+}$-co-doped SZB glasses but also the optimal molar concentration of Mn^{2+} ions in the $MnCO_3$ compound such that the BFN_NIR emission of $Er^{3+}/Tm^{3+}/Yb^{3+}$-co-doped SZB glasses is a maximum. In addition, the role of Mn^{2+} ions in the $MnCO_3$ compound in reducing the gain coefficient for the $^4I_{13/2} \rightarrow \,^4I_{15/2}$ transition of Er^{3+} ions was also examined. The obtained results are able to guide the selection of more optimal materials for EDFA and TDFA optical amplifiers.

2. Experimental details

2.1. Materials

In this experiment, the glass materials are fabricated by the conventional melting method. All the raw materials consisting of SiO_2, ZnO, BaO, TiO_2, $MnCO_3$, Er_2O_3, Tm_2O_3, and Yb_2O_3 used in this study are laboratory reagents with high purity (99.99%).

The abbreviations, chemical compositions, and detailed molar ratios are listed in Table 1.

2.2. Experimental methods

Approximately 12 g of the mixtures of raw materials were weighed for each glass sample using an electronic analytical balance. After being finely ground using an onyx mortar and pestle, these mixtures were compressed into a platinum crucible and were then heated in a German-manufactured Nabertherm electric furnace at 1580 °C for a continuous period of 50 minutes, under an air atmosphere.[23] In the process of fabrication of the host glass and the glass doped with rare earth elements, the raw material mixtures after fine grinding are often heated at a temperature that is equal to or greater than the glass transition temperature of the raw materials, (abbreviated T_g). This temperature T_g is related to the melting point temperature of the materials (T_m) through the expression $T_g = \frac{2}{3}T_m$.[24,25] In the experiment in this study, the SiO_2, ZnO, TiO_2, BaO, Er_2O_3, Tm_2O_3, and Yb_2O_3 raw material mixtures have melting points greater than 1580 °C. However, we chose the material melting temperature of 1580 °C[23] at which these material mixtures are melted enough to form glasses.[23,24] In the next step, the melted mixtures were poured into a mold and quenched on the surface of a stainless steel plate to form the raw glass. To increase the mechanical strength and remove thermal strain from the raw glass, all raw glass samples were annealed at ~500 °C for a continuous period of 12 hours.[17,19,23,26] The glass samples used for optical measurements were cut to a size of ~10 mm × 10 mm × 2 mm. The edges and surfaces of these glass samples were then thoroughly polished.

Table 1 Detailed chemical composition and concentration ratios of SiO_2–ZnO–BaO–TiO_2–Er_2O_3–Tm_2O_3–$MnCO_3$–Yb_2O_3 barium zinc silicate glasses

Name of glass sample	Details of composition and molar concentration (in mol%)							
	SiO_2	ZnO	BaO	TiO_2	Er_2O_3	Tm_2O_3	$MnCO_3$	Yb_2O_3
SZB-2Mn2Yb	45	26	17	8	0	0	2	2
SZB-0.5Er	45	26	20.5	8	0.5	0	0	0
SZB-1Tm	45	26	20	8	0	1	0	0
SZB-0.5Er2Yb	45	26	18.5	8	0.5	0	0	2
SZB-0.5Er2Yb2Mn	45	26	16.5	8	0.5	0	2	2
SZB-0.5Er2Yb2.5Mn	45	26	16	8	0.5	0	2.5	2
SZB-0.5Er2Yb3Mn	45	26	15.5	8	0.5	0	3	2
SZB-0.5Er2Yb3.5Mn	45	26	15	8	0.5	0	3.5	2
SZB-0.5Er2Yb4Mn	45	26	14.5	8	0.5	0	4	2
SZB-1Tm2Yb	45	26	18	8	0	1	0	2
SZB-1Tm2Yb2Mn	45	26	16	8	0	1	2	2
SZB-1Tm2Yb2.5Mn	45	26	15.5	8	0	1	2.5	2
SZB-1Tm2Yb3Mn	45	26	15	8	0	1	3	2
SZB-1Tm2Yb3.5Mn	45	26	14.5	8	0	1	3.5	2
SZB-1Tm2Yb4Mn	45	26	14	8	0	1	4	2
SZB-0.5Er1Tm2Yb	45	26	17.5	8	0.5	1	0	2
SZB-0.5Er21TmYb2Mn	45	26	15.5	8	0.5	1	2	2
SZB-0.5Er1Tm2Yb2.5Mn	45	26	15	8	0.5	1	2.5	2
SZB-0.5Er1Tm2Yb3Mn	45	26	14.5	8	0.5	1	3	2
SZB-0.5Er1Tm2Yb3.5Mn	45	26	14	8	0.5	1	3.5	2
SZB-0.5Er1Tm2Yb4Mn	45	26	13.5	8	0.5	1	4	2

The EDS spectrum was carried out using field emission scanning electron microscopy (FE-SEM), with a Jeol JSM-6510LV. Optical transmittance spectra of the glass within the wavelength range of 350 to 2000 nm were carried out using a Hitachi U-4100 UV/VIS/NIR spectrophotometer. NIR emission spectra of the glass within the wavelength range of 1300 to 2100 nm were measured using a Zolix SBP300 spectrophotometer with an InGaAs detector under excitation by a 980 nm LD. Optical transmittance and NIR emission spectra measurements as well as EDS analysis of the glass samples were performed at ambient temperature.[17,19]

3. Results and discussion

3.1. EDS analysis

To determine whether the elements in the original raw material still exist in the glass materials after fabrication, we conducted an EDS analysis for the SZB-0.5Er1Tm2Yb2Mn glass sample, and the analyzed results within the energy range from 0 to 10 keV are plotted in Fig. 1. The energy levels of each element are listed in detail in Table 2. The obtained results of the EDS spectrum analysis of the SZB-0.5Er1Tm2Yb2Mn glass sample confirmed that the C, Ti, O, Ba, Zn, Si, Mn, Tm, Er, and Yb elements were still present in the SiO_2–ZnO–BaO–TiO_2–Er_2O_3–Tm_2O_3–$MnCO_3$–Yb_2O_3 glass matrix.[27,28] It should be noted that

Fig. 1 EDS spectral analysis of the SZB-0.5Er1Tm2Yb2Mn glass sample.

the Mn element has many different valence states, including +2, +3, +4, +5, +6, and +7 valences. When the $MnCO_3$ compound is introduced into the host glasses, the Mn element exists almost exclusively in the Mn 2p1 and Mn 2p3 valence states and this was investigated through XPS analysis and reported in a previous study.[17] Following the results achieved on the behavior of the $MnCO_3$ compound doped into barium zinc silicate glasses, the goal of this work is mainly to focus on investigating the role of Mn^{2+} ions in the $MnCO_3$ compound for combining to form an Mn^{2+}–Yb^{3+} dimer and transferring energy to Er^{3+} and Tm^{3+} ions to enhance the NIR emission intensity of Er^{3+}/Tm^{3+}/Yb^{3+}-co-doped barium zinc silicate glasses under 980 nm LD excitation.

3.2. Optical transmittance spectra

In Fig. 2(A), optical transmittance spectra of the SZB-0.5Er, SZB-0.5Er2Yb2Mn, SZB-1Tm, and SZB-1Tm2Yb2Mn glass samples are shown in curves (a), (b), (c) and (d), respectively. Curve (a) shows the optical transmittance spectra of the Er^{3+}-doped sample in which seven optical transmittance bands can be observed corresponding to the $^4I_{15/2} \rightarrow {}^4G_{11/2}$, -$^4F_{7/2}$, -$^2H_{11/2}$, -$^4S_{3/2}$, -$^4F_{9/2}$, -$^4I_{11/2}$ and -$^4I_{13/2}$ transitions of Er^{3+} ions.[29,30] Curve (b) shows the optical transmittance spectrum of the Er^{3+}/Yb^{3+}/Mn^{2+}-co-doped sample in which nine optical transmittance bands can be observed, among which, one corresponds to the $^6A_{1g} \rightarrow {}^4T_{1g}$ transition of Mn^{2+} ions,[13,14,17] one corresponds to the $^2F_{7/2} \rightarrow {}^2F_{5/2}$ transition of Yb^{3+} ions,[27,28] and the remaining seven correspond to the $^4I_{15/2} \rightarrow {}^4G_{11/2}$, -$^4F_{7/2}$, -$^2H_{11/2}$, -$^4S_{3/2}$, -$^4F_{9/2}$, -$^4I_{11/2}$ and -$^4I_{13/2}$ transitions of Er^{3+} ions.[30,31] Curve (c) shows the optical transmittance spectra of the Tm^{3+}-doped in SZB-1Tm glass sample in which five optical transmittance bands can be observed corresponding to the $^3H_6 \rightarrow {}^1G_4$, -$^3F_{2,3}$, -$^3H_4$, -$^3H_5$, and -$^3F_4$ transitions of Tm^{3+} ions. Curve (d) shows the optical transmittance spectra of the Tm^{3+}/Yb^{3+}/Mn^{2+} co-doped in SZB-1Tm2Yb2Mn glass sample in which seven optical transmittance bands can be observed, among which, one corresponds to the $^6A_{1g} \rightarrow {}^4T_{1g}$ transition of Mn^{2+} ions,[13,14,17] one corresponds to the $^2F_{7/2} \rightarrow {}^2F_{5/2}$ transition of Yb^{3+} ions,[27,28,31] and the remaining five optical transmittance bands correspond to the $^3H_6 \rightarrow {}^1G_4$, -$^3F_{2,3}$, -$^3H_4$, -$^3H_5$, and -$^3F_4$ transitions of Tm^{3+} ions.[27,28]

To more clearly observe the optical transmittance spectra of Er^{3+}, Mn^{2+}, and Yb^{3+} ions, we measured and further analyzed the optical transmittance spectra of the SZB-2Mn2Yb, SZB-0.5Er1Tm2Yb, and SZB-0.5Er1Tm2Yb2Mn glass samples. The analyzed results of these optical transmittance spectra are plotted in Fig. 2(B). The obtained results displayed in curve (c)

Table 2 Details of the energy levels of the elements in the EDS spectral analysis

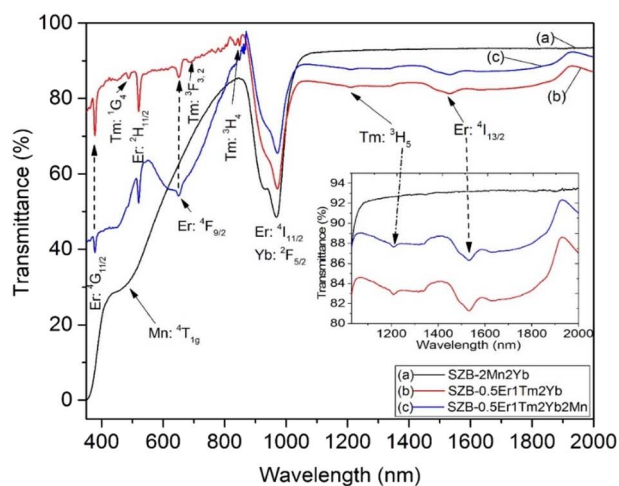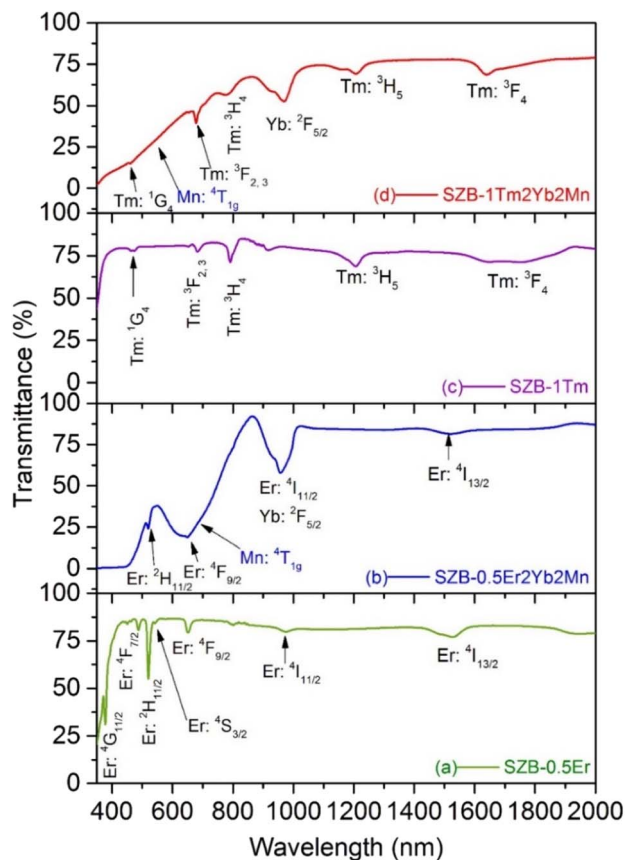| Energy	Element									
	C	Ti	O	Ba	Zn	Si	Mn	Er	Tm	Yb
L_α (keV)	0.278	0.452	0.526	0.971	1.012	1.741	0.638	1.405	7.179	1.521
K_α (keV)		4.509		4.466	8.629		5.895	6.946		7.415

Fig. 2 (A) Optical transmittance spectra of the SZB-0.5Er, SZB-0.5Er2Yb2Mn, SZB-1Tm, and SZB-1Tm2Yb2Mn glass samples. (B) Optical transmittance spectra of the SZB-2Mn2Yb, SZB-0.5Er1Tm2Yb, and SZB-0.5Er1Tm2Yb2Mn glass samples.

of Fig. 2(B) indicate that we can also observe all nine optical transmittance bands corresponding to $^6A_{1g} \rightarrow {}^4T_{1g}$ of Mn^{2+} ions, $^2F_{7/2} \rightarrow {}^2F_{5/2}$ of Yb^{3+} ions,[4,11,13,14,17] and the $^4I_{15/2} \rightarrow {}^4G_{11/2}$, $^4F_{7/2}$, $^2H_{11/2}$, $^4S_{3/2}$, $^4F_{9/2}$, $^4I_{11/2}$, $^4I_{13/2}$ transitions of Er^{3+} ions,[4,30,31] similar to the analysis above. Interestingly, the analyzed results reveal that the transmittance spectrum of the SZB-0.5Er1Tm2Yb2Mn glass samples containing Mn^{2+}

components in the wavelength region of ~380–900 nm was decreased whereas the optical transmittance spectrum in the wavelength region of ~900–2000 nm was increased compared to SZB-0.5Er1Tm2Yb glass samples without Mn^{2+} components. Also from the results displayed in Fig. 2(B), it can be seen that the optical transmittance spectrum of the SZB-2Mn2Yb glass sample within the wavelength range ~1000–2000 nm is higher than that of the SZB-0.5Er1Tm2Yb or SZB0.5Er1Tm2Yb2Mn glass samples. For the SZB-0.5Er1Tm2Yb and SZB0.5Er1Tm2Yb2Mn glass samples, in addition to the Mn^{2+} and Yb^{3+} components, there are also Er^{3+} and Tm^{3+} components with absorption peaks at about 1230 nm and 1542 nm in the wavelength range ~1000 to 2000 nm, corresponding to the $^3H_6 \rightarrow {}^3H_5$ transition of Tm^{3+} ions and the $^4I_{15/2} \rightarrow {}^4I_{13/2}$ transition of Er^{3+} ions, respectively. Part of the excitation energy is thus absorbed in the wavelength region from ~1000 to 2000 nm, which does not occur for the SZB-2Mn2Yb glass sample. This is the reason why the transmittance spectrum of the SZB-2Mn2Yb sample is higher than those of the other glass samples.

3.3. NIR emission spectra

NIR emission spectra of the SZB-0.5Er2YbxMn (x = 0, 2, 2.5, 3, 3.5, and 4 mol%) glass samples under 980 nm LD excitation are plotted in Fig. 3. For the SZB-0.5Er2Yb glass sample, the NIR emission of Er^{3+}/Yb^{3+}-co-doped peaks at ~1542 nm corresponds to the $^4I_{13/2} \rightarrow {}^4I_{15/2}$ transition of Er^{3+}. With the increased concentrations of the $MnCO_3$ compound from 2 up to 4 mol%, the NIR emission intensity of the Er^{3+}/Yb^{3+}-co-doped peaks at ~1542 nm was significantly increased. Moreover, the NIR emission peak of Er^{3+} tends to split and shift the peaks by $\Delta\lambda = 1553 - 1542$ nm = 11 nm. The main reason for the increase in NIR emission intensity of Er^{3+}/Yb^{3+}-co-doped peaks at ~1542 nm can be attributed to the combination between Yb^{3+} and Mn^{2+} ions in the $MnCO_3$ compound leading to the formation of Mn^{2+}–Yb^{3+} dimers[13,32] contributing to the energy transfer (ET) to the $^4I_{13/2} \rightarrow {}^4I_{15/2}$ transition of Er^{3+} ions.[13,23] The
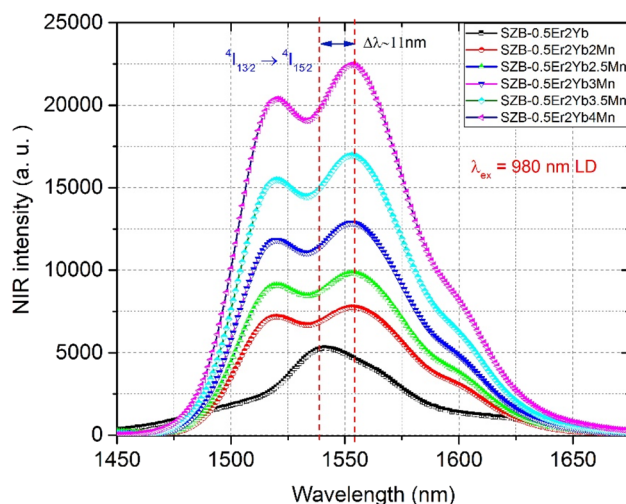

Fig. 3 NIR emission spectra of the SZB-0.5Er2YbxMn (x = 0, 2, 2.5, 3, 3.5, and 4 mol%) glass samples.

formation of an Mn^{2+}–Yb^{3+} dimer can be interpreted with the result shown in Fig. 3, where the Er^{3+} and Yb^{3+} concentrations are unchanged when the concentration of the $MnCO_3$ compound increases from 2 up to 4 mol%, and the NIR emission intensity of the Er^{3+}/Yb^{3+}-co-doped peaks at ~1542 nm under the excitation of 980 nm LD was significantly increased. However, the Mn^{2+} ions cannot receive the direct excitation of the 980 nm LD, proving that Mn^{2+} ions combine with the Yb^{3+} ions to form an Mn^{2+}–Yb^{3+} dimer,[13,23] and therefore, the Mn^{2+}–Yb^{3+} dimers receive the excitation of the 980 nm LD and transfer energy from the Mn^{2+}–Yb^{3+} dimer to the $^4I_{13/2} \rightarrow \, ^4I_{15/2}$ transition of Er^{3+} ions.[13,23] The addition of $MnCO_3$ compound into the host glass efficiently promotes not only the formation of the Mn^{2+}–Yb^{3+} dimer but also contributes to breaking of the O–Zn, Si–O, Si–O–Si, Zn–O–Zn, and Si–O–Zn bonds,[33] subsequently creating new non-bridging oxygens (NBOs), like Mn–O, Mn–Si, Si–O–Mn, Mn–O–Mn, and Mn–O–Zn bonds.[34,35] Therefore, we believe that the presence of Mn^{2+} ions in the $MnCO_3$ compound contributed to shifting the NIR emission peak at the $^4I_{13/2} \rightarrow \, ^4I_{15/2}$ transition of Er^{3+} ions.

We also investigated the effects of Mn^{2+} on the NIR emission bandwidth flatness (NIR_EBF) parameter of Er^{3+}/Yb^{3+} co-doped in SZB glasses. The NIR_EBF parameter of Er^{3+}/Yb^{3+} co-doped in SZB glasses can be calculated based on the NIR emission spectra of Er^{3+}/Yb^{3+} co-doped in SZB glasses with the following formula:[19,23]

$$\text{NIR\_EBF} = \frac{\sqrt[N]{\prod_{n=0}^{N-1} I(n)}}{\frac{\sum_{n=0}^{N-1} I(n)}{N}} = \frac{\exp\left(\frac{1}{N} \sum_{n=0}^{N-1} \ln I(n)\right)}{\frac{1}{N} \sum_{n=0}^{N-1} I(n)} \quad (1)$$

where $I(n)$ is the NIR emission intensity of Er^{3+}/Yb^{3+} co-doped in SZB glasses within the analytical data range n of the NIR emission wavelength N.[19,23] NIR_EBF takes a value from 0 to

1.[19,23] The value of NIR_EBF is equal to 1 when all values of $I(n)$ are equal.[19,23] The NIR_EBF calculated results of Er^{3+}/Yb^{3+} co-doped in SZB glasses displayed in Fig. 4 show that with increasing concentrations of Mn^{2+} ions, the NIR_EBF of Er^{3+}/Yb^{3+} co-doped in SZB glasses gradually decreased.

Similarly, the NIR emission spectra of SZB-1Tm2YbxMn (x = 0, 2, 2.5, 3, 3.5, and 4 mol%) glass samples under excitation of 980 nm LD are plotted in Fig. 5 and indicate that the NIR emission of the Tm^{3+}/Yb^{3+}-co-doped sample has two peaks at about ~1457 and ~1801 nm, corresponding to the $^3H_4 \rightarrow \, ^3F_4$ and $^3F_4 \rightarrow \, ^3H_6$ transitions of Tm^{3+} ions.[36,37] Along with the increase in $MnCO_3$ concentration from 2 up to 4 mol%, the NIR emission intensity of Tm^{3+}/Yb^{3+}-co-doped peaks at ~1457 and ~1801 nm was also significantly increased. This result is due to the ET processes from the Mn^{2+}–Yb^{3+} dimer to the $^3H_4 \rightarrow \, ^3F_4$ and $^3F_4 \rightarrow \, ^3H_6$ transitions of Tm^{3+} ions.[17]

Formula (1) continued to be used to calculate the NIR_EBF spectra of Tm^{3+}/Yb^{3+}-co-doped samples when the molar concentration of the $MnCO_3$ compound increases from 0 up to 4 mol% and the results of the calculation are shown in the insert to Fig. 5. These results show that the NIR_EBF spectra of the Tm^{3+}/Yb^{3+}-co-doped sample reached the optimal value of 0.668 when the molar concentration of the $MnCO_3$ compound was 2 mol%. Energy levels of Er^{3+}, Tm^{3+}, Yb^{3+} ions, the Mn^{2+}–Yb^{3+} dimer and mechanisms of the ET_I (I = 1, 2, 3, 4, and 5) processes in the SZB glass system are shown in Fig. 6. Mechanisms of the ET_I (I = 1, 2, 3, 4, and 5) processes between the Mn^{2+}–Yb^{3+} dimer with Er^{3+}, Tm^{3+} ions were also reported and discussed in detail in our previous studies.[17,26] These ET_I (I = 1, 2, 3, 4, and 5) processes can be described in detail in the form of the following equations:

$$ET_1: \, ^2F_{5/2}(Yb^{3+}) + \, ^3H_5(Tm^{3+}) \rightarrow \, ^2F_{7/2}(Yb^{3+}) + \, ^3H_6(Tm^{3+}).[17]$$

$$ET_2: |^2F_{5/2}, \, ^6A_1\rangle(Mn^{2+}\text{–}Yb^{3+}) + \, ^3H_5(Tm^{3+}) \rightarrow$$
$$|^2F_{7/2}, \, ^6A_1\rangle(Mn^{2+}\text{–}Yb^{3+}) + \, ^3H_6(Tm^{3+}).[17]$$
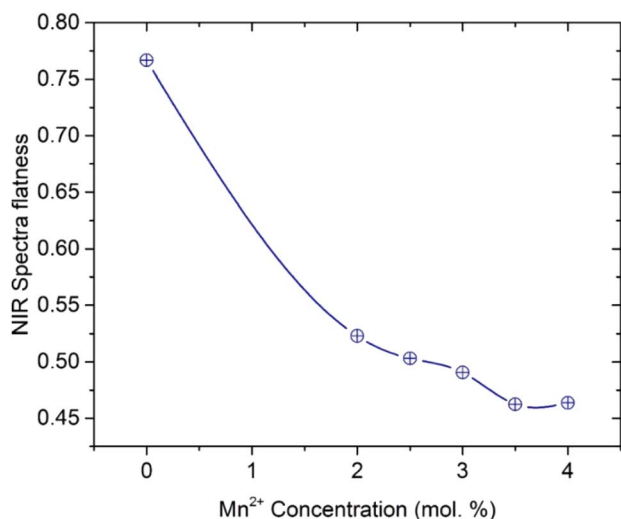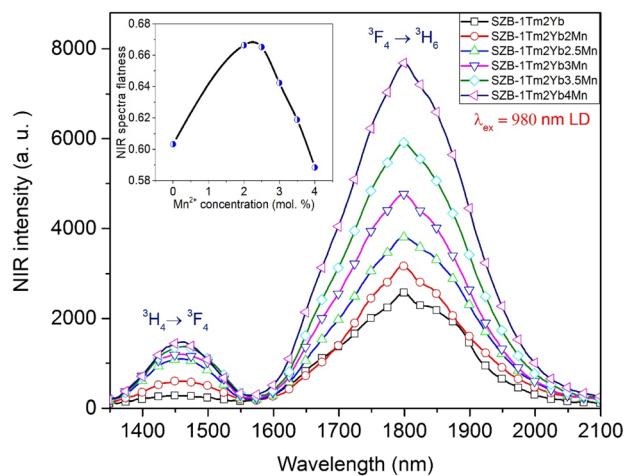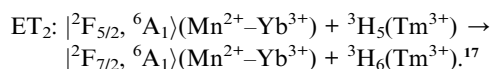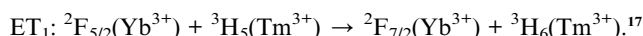

Fig. 4 Relationship between NIR spectra flatness of the SZB-0.5Er2YbxMn (x = 0, 2, 2.5, 3, 3.5, and 4 mol%) glass samples and molar concentration of Mn^{2+} ions.

Fig. 5 NIR emission spectra of the SZB-1Tm2YbxMn (x = 0, 2, 2.5, 3, 3.5, and 4 mol%) glass samples.
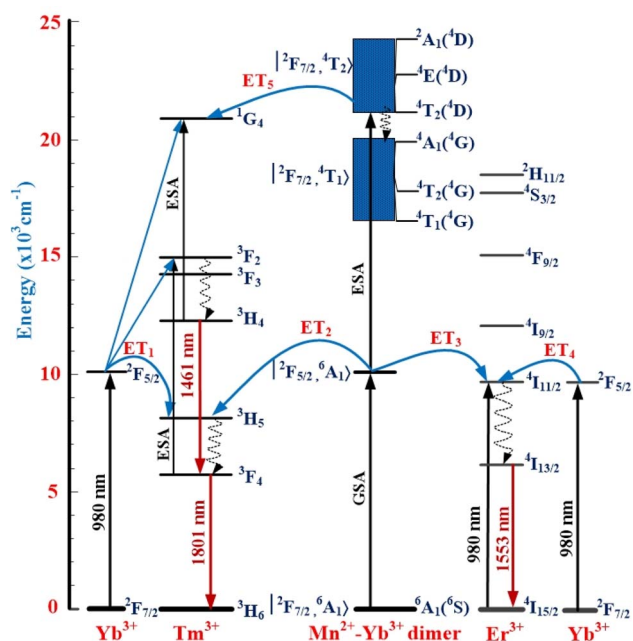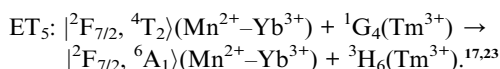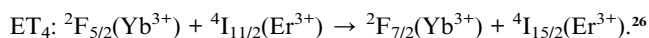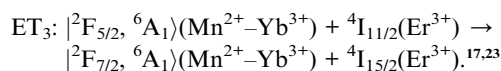
Fig. 6 Energy levels of Er^{3+}, Tm^{3+}, Yb^{3+}, $Mn^{2+}-Yb^{3+}$ dimer and mechanisms of ET_l ($l = 1, 2, 3, 4,$ and 5) processes in the SZB glass system.

$$ET_3: |{}^2F_{5/2}, {}^6A_1\rangle(Mn^{2+}-Yb^{3+}) + {}^4I_{11/2}(Er^{3+}) \rightarrow$$
$$|{}^2F_{7/2}, {}^6A_1\rangle(Mn^{2+}-Yb^{3+}) + {}^4I_{15/2}(Er^{3+}).^{17,23}$$

$$ET_4: {}^2F_{5/2}(Yb^{3+}) + {}^4I_{11/2}(Er^{3+}) \rightarrow {}^2F_{7/2}(Yb^{3+}) + {}^4I_{15/2}(Er^{3+}).^{26}$$

$$ET_5: |{}^2F_{7/2}, {}^4T_2\rangle(Mn^{2+}-Yb^{3+}) + {}^1G_4(Tm^{3+}) \rightarrow$$
$$|{}^2F_{7/2}, {}^6A_1\rangle(Mn^{2+}-Yb^{3+}) + {}^3H_6(Tm^{3+}).^{17,23}$$

To achieve one of the main goals of this study, we investigated the effects of Mn^{2+} ions in the $MnCO_3$ compound on the NIR_EBF spectra of $Er^{3+}/Tm^{3+}/Yb^{3+}$-co-doped SZB glasses. We kept the molar compositions of the $Er^{3+}/Tm^{3+}/Yb^{3+}$-co-doped
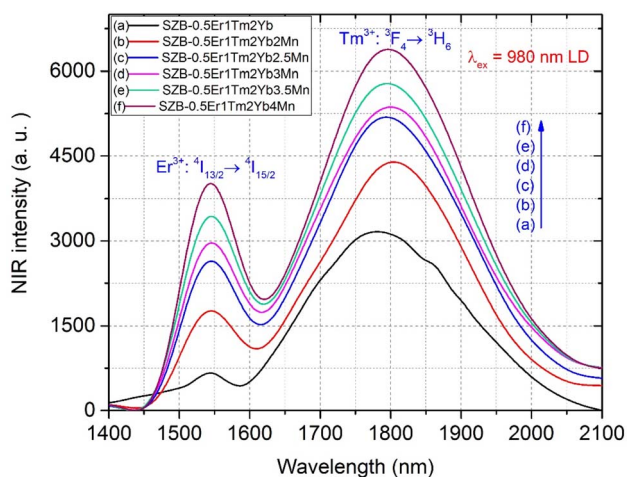

Fig. 7 NIR emission spectra of the SZB-0.5Er1Tm2YbxMn ($x = 0, 2, 2.5, 3, 3.5,$ and 4 mol%) glass samples.
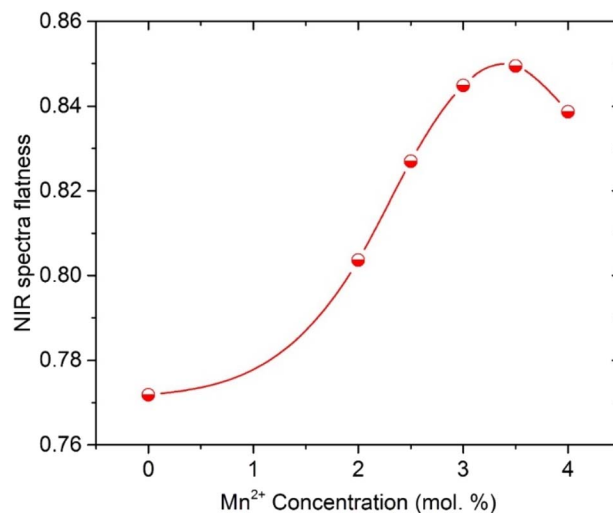

Fig. 8 The relationship between the molar concentration of Mn^{2+} ions and NIR_EBF parameter of the SZB-0.5Er1Tm2YbxMn ($x = 0, 2, 2.5, 3, 3.5,$ and 4 mol%) glass samples.

sample to $0.5Er^{3+}/1Tm^{3+}/2Yb^{3+}$, and changed the molar composition of the $MnCO_3$ compound from 2 up to 4 mol%. As shown in Fig. 7, the NIR emission spectra of SZB-0.5Er1T-m2YbxMn ($x = 0, 2, 2.5, 3, 3.5,$ and 4 mol%) glass samples under excitation by a 980 nm LD reveal that when the molar concentration of the $MnCO_3$ compound increases from 2 up to 4 mol%, the NIR emission intensity of the $Er^{3+}/Tm^{3+}/Yb^{3+}$-co-doped peaks at ~1553 and ~1801 nm also strongly increases. This result may be due to $Mn^{2+}-Yb^{3+}$ dimers being formed during the excitation by 980 nm LD, with the energies from Mn^{2+} ions and $Mn^{2+}-Yb^{3+}$ dimers simultaneously transferred to Er^{3+} and Tm^{3+} ions. The NIR emission spectra of $Er^{3+}/Tm^{3+}/Yb^{3+}$ co-doped in the SZB-0.5Er1Tm2YbxMn ($x = 0, 2, 2.5, 3, 3.5,$ and 4 mol%) glass under 980 nm LD excitation created an NIR bandwidth of ~430 nm. The NIR_EBF spectra of the $Er^{3+}/Tm^{3+}/Yb^{3+}$-co-doped samples were determined when the molar concentration of Mn^{2+} ions in the $MnCO_3$ compound increased from 2 up to 4 mol% using formula (1). The results of the calculation of the NIR_EBF value, given in Fig. 8, showed that the NIR_EBF spectra of the $Er^{3+}/Tm^{3+}/Yb^{3+}$-co-doped sample reached the optimal value of 0.849 when the molar concentration of Mn^{2+} ions in the $MnCO_3$ compound was 3.5 mol%.

3.4. Cross-section and gain coefficient study

To evaluate the influence of Mn^{2+} ions in the $MnCO_3$ compound on the gain coefficient of Er^{3+} ($G_{Er}(\lambda)$), we first investigated and calculated the absorption cross-section $\sigma_{abs}(\lambda)$ and emission cross-section $\sigma_{ems}(\lambda)$ for the ${}^4I_{13/2} \rightarrow {}^4I_{15/2}$ transition of Er^{3+} ions in the SZB glasses based on McCumber's theory.[6,38,39] The value of $\sigma_{abs}(\lambda)$ is calculated from the absorbance spectrum according to the following formula:[6,38,39]

$$\sigma_{abs}(\lambda) = \frac{2.303}{Cd} A(\lambda), \tag{2}$$

in which $A(\lambda)$ is the absorbance spectrum; λ is the wavelength; C is the concentration of Er^{3+} ions; and d is the thickness of the

SZB glass samples, where the glass sample in this study has a thickness of $d = 2$ mm.[6,38] The absorbance spectrum $A(\lambda)$ can be calculated from the transmittance spectrum $T(\lambda)$ according to the formula:[40,41]

$$A(\lambda) = -\log_{10} T(\lambda) = 2 - \log_{10}(\% \ T(\lambda)), \quad (3)$$

where $\% \ T(\lambda)$ is the transmittance spectrum (measured as a percentage) determined from the experimental results in Fig. 2(A) and (B).

The value of $\sigma_{ems}(\lambda)$ is thus determined in relation to the value of $\sigma_{abs}(\lambda)$ as follows:[6,39]

$$\sigma_{ems}(\lambda) = \sigma_{abs}(\lambda) \frac{Z_L}{Z_U} \exp\left(\frac{hc}{kT}\left(\frac{1}{\lambda_{UL}} - \frac{1}{\lambda}\right)\right), \quad (4)$$

where Z_U and Z_L are the partition functions of the upper and lower manifolds, respectively; T is the temperature; h is Planck's constant; k is Boltzmann's constant; c is the speed of light; λ is the photon wavelength; λ_{UL} the wavelength corresponding to the transition between the bottom of the excited (upper) state manifold and the bottom of the ground (lower) state manifold.[6,35,36] The value of $\sigma_{abs}(\lambda)$ for the $^4I_{15/2} \rightarrow {}^4I_{13/2}$ transition and of $\sigma_{ems}(\lambda)$ for the $^4I_{13/2} \rightarrow {}^4I_{15/2}$ transition of Er^{3+} ions are determined as shown in Fig. 9. The gain coefficient $G(\lambda)$ for transitions of the REIs in the glass samples can be determined with the following formula:[6,38,39]

$$G(\lambda) = C \cdot [P \cdot \sigma_{ems}(\lambda) - (1 - P) \cdot \sigma_{abs}(\lambda)], \quad (5)$$

in which P is the population inversion and $P = 0$–1 stands for the ratio between the number of REIs in the excited state to the total number of REIs.

Formulae (2)–(5) are used to determine the values of $\sigma_{abs}(\lambda)$, $\sigma_{ems}(\lambda)$, and $G_{Er}(\lambda)$, respectively, for the $^4I_{13/2} \rightarrow {}^4I_{15/2}$ transition of Er^{3+} ions in the SZB-0.5Er glass sample. The values of $G_{Er}(\lambda)$ were calculated and are shown in Fig. 10. We can observe that the $G_{Er}(\lambda)$ value becomes positive in the range wavelength of ~1500–1600 nm for cases where P is equal to 0.5 to 1. When P is
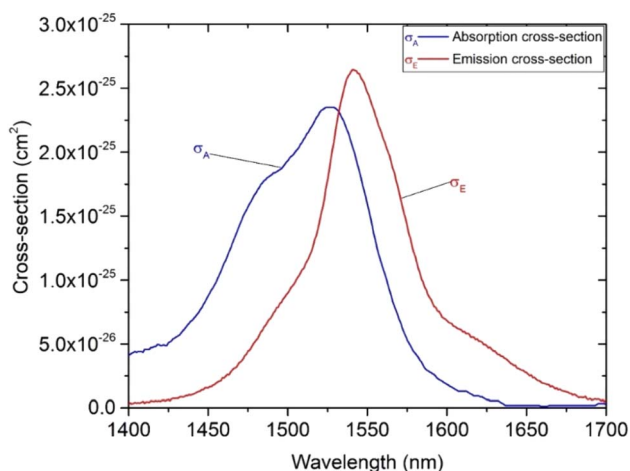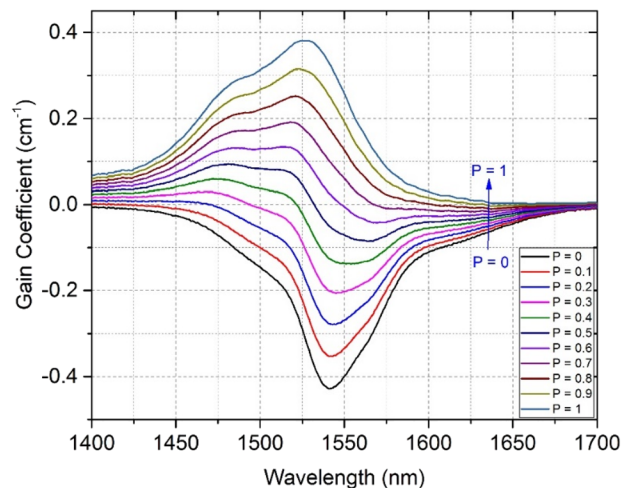

Fig. 10 Gain coefficient for the $^4I_{13/2} \rightarrow {}^4I_{15/2}$ transition of Er^{3+} ions in the SZB-0.5Er glass sample.

greater than 0.6, the NIR emission of the Er^{3+}-doped SZB-0.5Er glass sample exhibits a flat net gain covering the L-, U-, and (L + U)-bands.[6] At the same time, the $G_{Er}(\lambda)$ value is found to be about 0.38, corresponding to $P = 1$. Similarly, we also used formulae (2)–(5) to determine the values of $\sigma_{abs}(\lambda)$, $\sigma_{ems}(\lambda)$, and $G_{Er\_Mn}(\lambda)$, respectively, for the $^4I_{13/2} \rightarrow {}^4I_{15/2}$ transition of Er^{3+} ions in the SZB-0.5Er2Yb2Mn glass sample. The values of $\sigma_{abs}(\lambda)$ and $\sigma_{ems}(\lambda)$ of the SZB-0.5Er2Yb2Mn glass sample are shown in Fig. 11 and the values of $G_{Er\_Mn}(\lambda)$ for the $^4I_{13/2} \rightarrow {}^4I_{15/2}$ transition of Er^{3+} ions in the SZB-0.5Er2Yb2Mn glass sample are shown in Fig. 12. Comparison of the results in Fig. 10 and 12 shows that with the existence of Mn^{2+} ions in the SZB-0.5Er2Yb2Mn glass sample, the value of $G_{Er\_Mn}(\lambda)$ for the $^4I_{13/2} \rightarrow {}^4I_{15/2}$ transition of Er^{3+} ions was significantly reduced. The value of $G_{Er\_Mn}(\lambda)$ is found to be about 0.21 corresponding to $P = 1$. These $G_{Er\_Mn}(\lambda)$ and $G_{Er}(\lambda)$ calculation results showed that in the presence of Mn^{2+} ions and an Mn^{2+}–Yb^{3+} dimer, the broadband NIR emission of the $^4I_{13/2} \rightarrow {}^4I_{15/2}$ transition of Er^{3+}

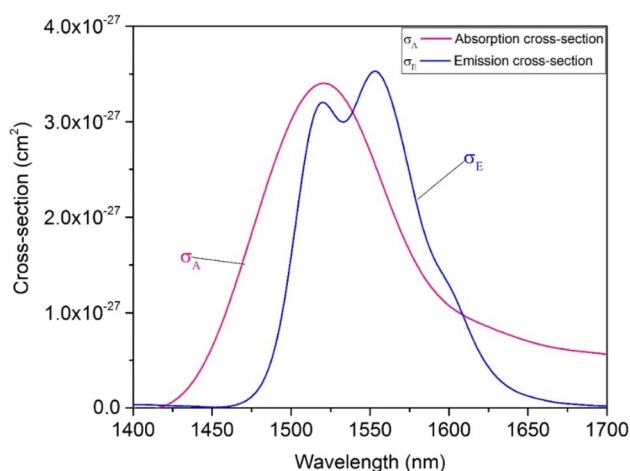Fig. 9 Absorption and emission cross-sections of the SZB-0.5Er glass sample.

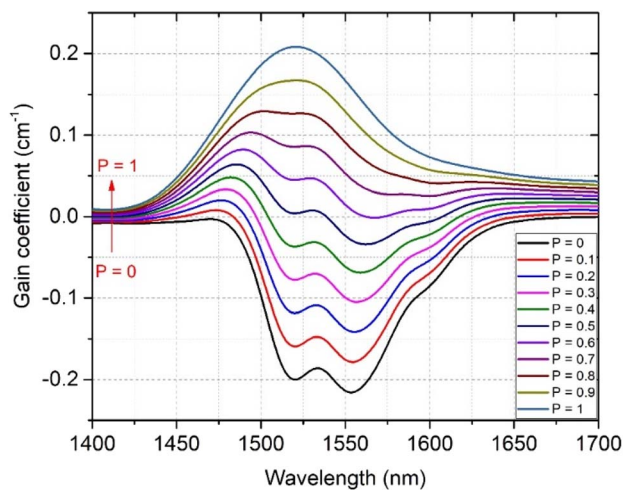Fig. 11 Absorption and emission cross-sections of the SZB-0.5Er2Yb2Mn glass sample.

Fig. 12 Gain coefficient for the $^4I_{13/2} \rightarrow {}^4I_{15/2}$ transition of Er^{3+} ions in the SZB-0.5Er2Yb2Mn glass sample.

ions in this study can be utilized for optical amplifiers. The γ_G ratio between $G_{Er\_Mn}(\lambda)$ and $G_{Er}(\lambda)$ is determined as follows:

$$\gamma_G = \frac{G_{Er\_Mn}(\lambda)}{G_{Er}(\lambda)} = \frac{0.21}{0.38} = 0.553 \qquad (6)$$

Based on the above results and analyses, we can confirm that in the presence of Mn^{2+} ions, the NIR bandwidth flatness of Er^{3+} ions was improved, but the gain coefficient for the $^4I_{13/2} \rightarrow {}^4I_{15/2}$ transition of Er^{3+} ions was significantly reduced. Therefore, depending on the specificity of the application in the optical amplifier, we should choose the type of SZB glass material with or without the Mn^{2+} component to suit the specific applications.

4. Conclusions

In this work, the effects of Mn^{2+} ions in the $MnCO_3$ compound leading to the formation of an Mn^{2+}–Yb^{3+} dimer and affecting the gain coefficient for the $^4I_{13/2} \rightarrow {}^4I_{15/2}$ transition of Er^{3+} ions and the NIR_EBF value of Er^{3+}-doped and $Er^{3+}/Tm^{3+}/Yb^{3+}$-co-doped barium zinc silicate glasses under 980 nm LD excitation were investigated. A broadband NIR emission of $Er^{3+}/Tm^{3+}/Yb^{3+}$-co-doped barium zinc silicate glasses with an FWHM of ~430 nm was observed. The roles of Mn^{2+} ions in the $MnCO_3$ compound led to the formation of an Mn^{2+}–Yb^{3+} dimer and contributed to a significant increase in the NIR_EBF value of Er^{3+}-doped and $Er^{3+}/Tm^{3+}/Yb^{3+}$-co-doped barium zinc silicate within the NIR wavelength range of 1600–2200 nm. The NIR_EBF value of $Er^{3+}/Tm^{3+}/Yb^{3+}$-co-doped SZB glasses obtained at 0.849 corresponds to the molar concentration of $MnCO_3$ compound of 3.5 mol%. However, the presence of Mn^{2+} ions in the SZB glass composition also led to a significant decrease in the gain coefficient for the $^4I_{13/2} \rightarrow {}^4I_{15/2}$ transition of Er^{3+} ions. The results obtained in this study will be able to guide the selection of glass material compositions for applications in optical amplifiers in the future.

Conflicts of interest

There are no conflicts of interest to declare.

Acknowledgements

References

1 H. K. Dan, N. M. Ty, V. H. Nga, D. T. Phuc, A.-L. Phan, D. C. Zhou and J. B. Qiu, Broadband flat near-infrared emission and energy transfer of Pr^{3+}–Er^{3+}–Yb^{3+} tri-doped niobate tellurite glasses, *J. Non-Cryst. Solids*, 2020, **549**, 120335, DOI: **10.1016/j.jnoncrysol.2020.120335**.

2 D. C. Zhou, R. F. Wang, Z. W. Yang, Z. G. Song, Z. Y. Yin and J. B. Qiu, Spectroscopic properties of Tm^{3+} doped TeO_2–R_2O–La_2O_3 glasses for 1.47 μm optical amplifiers, *J. Non-Cryst. Solids*, 2011, **357**, 2409–2412, DOI: **10.1016/j.jnoncrysol.2010.12.027**.

3 S. M. Li, L. H. Zhang, X. J. Tan, W. Deng, M. Z. He, G. Z. Chen, M. Xu, Y. L. Yang, S. L. Zhang, P. X. Zhang, Z. Q. Chen and Y. Hang, Growth, structure, and spectroscopic properties of a Tm^{3+}, Ho^{3+} co-doped Lu_2O_3 crystal for ~2.1 μm lasers, *Opt. Mater.*, 2019, **96**, 109277, DOI: **10.1016/j.optmat.2019.109277**.

4 P. X. Le, N. M. Ty, J. B. Qiu, D. C. Zhou and H. K. Dan, Enhanced upconversion and near-infrared emissions of co-doped Ho^{3+}/Yb^{3+} in TeO_2–ZnO–Na_2CO_3–La_2O_3 tellurite glasses, *Opt. Mater. Express*, 2019, **9**, 3998–4008, DOI: **10.1364/OME.9.003998**.

5 X. Wang, X. X. Jin, P. Zhou, X. L. Wang, H. Xiao and Z. J. Liu, High power, widely tunable, narrowband super fluorescent source at 2 μm based on a monolithic Tm-doped fiber amplifier, *Opt. Express*, 2015, **23**(3), 3382–3389, DOI: **10.1364/OE.23.003382**.

6 H. K. Dan, D.-N. Le, H. T. Nguyen-Truong, T. D. Tap, H. X. Vinh, N. M. Ty, R. F. Wang, D. C. Zhou and J. B. Qiu, Effects of Y^{3+} the enhancement NIR emission of Bi^+–Er^{3+} co-doped in transparent silicate glass-ceramics for Erbium-doped fiber amplifier (EDFA), *J. Lumin.*, 2020, **219**, 116942, DOI: **10.1016/j.jlumin.2019.116942**.

7 P. Peterka, I. Kašík, V. Matějec, W. Blanc, B. Faure, B. Dussardier, G. Monnom and V. Kubeček, Thulium-doped silica-based optical fibers for cladding-pumped fiber amplifiers, *Opt. Mater.*, 2007, **30**, 174–176, DOI: **10.1016/j.optmat.2006.11.039**.

8 Y. Guo, J. H. Xie, M. X. Yu, W. T. Huang, H. J. Yang, X. B. Li, L. X. Wang and Q. T. Zhang, The enhanced up-conversion green by Yb–Mn dimer in $NaBiF_4$: $Yb^{3+}/Er^{3+}/Mn^{2+}$ for optical fiber temperature sensor, *J. Alloys Compd.*, 2021, **888**, 161497, DOI: **10.1016/j.jallcom.2021.161497**.

9 L. Z. Xia, Y. Zhang, X. J. Shen and Y. X. Zhou, Broad and flat dual-band NIR luminescence from $Er^{3+}/Tm^{3+}/Ho^{3+}$ tri-doped

tellurite glass, *Opt. Lett.*, 2021, **46**(9), 2031–2034, DOI: **10.1364/OL.418971**.

10 N. Wang, R. J. Cao, M. Z. Cai, L. L. Shen, Y. Tian, F. F. Huang, S. Q. Xu and J. J. Zhang, Ho^{3+}/Tm^{3+} codoped lead silicate glass for 2 μm laser materials, *Opt. Laser Technol.*, 2017, **97**, 364–369, DOI: **10.1016/j.optlastec.2017.07.025**.

11 S. Ye, Y.-J. Li, D.-C. Yu, G.-P. Dong and Q.-Y. Zhang, Room-temperature upconverted white light from $GdMgB_5O_{10}$: Yb^{3+}, Mn^{2+}, *J. Mater. Chem.*, 2011, **21**, 3735–3739, DOI: **10.1039/C0JM03307C**.

12 S. Ye, E. H. Song, E. Ma, S. J. Zhang, J. Wang, X. Y. Chen, Q. Y. Zhang and J. R. Qiu, Broadband Cr^{3+}-sensitized upconversion luminescence in $La_3Ga_5GeO_{14}$: Cr^{3+}, Yb^{3+}, Er^{3+}, *Opt. Mater. Express*, 2014, **4**(4), 638–648, DOI: **10.1364/OME.4.000638**.

13 H. K. Dan, N. L. Thai, L. D. Tin, J. B. Qiu, D. C. Zhou and Q. Jiao, Enhanced near/mid-infrared emission bands centered at ~1.54 and ~2.73 μm of Er^{3+}-doped in transparent silicate glass-ceramics *via* $Mn^{2+}-Yb^{3+}$ dimer, *Infrared Phys. Technol.*, 2018, **95**, 33–38, DOI: **10.1016/j.infrared.2018.10.009**.

14 J. L. Wang, E. H. Song, M. Wu, W. B. Dai, S. Ye and Q. Y. Zhang, Selectively enhanced up- and down-conversion emissions of Er^{3+} *via* $Yb^{3+}-Mn^{2+}$ dimer sensitizing in spinel $MgGa_2O_4$: Er^{3+}, Yb^{3+}, Mn^{2+}, *Mater. Res. Bull.*, 2016, **74**, 340–345, DOI: **10.1016/j.materresbull.2015.10.043**.

15 X. X. Han, E. Song, S. Zhang, S. Ye, X. Yang and Q. Zhang, Heavy Mn^{2+} doped near-infrared photon upconversion luminescence in Fluoride $RbZnF_3$: Yb^{3+}, Mn^{2+} guided by dopant distribution simulation, *J. Mater. Chem. C*, 2020, **8**, 12164–12172, DOI: **10.1039/D0TC03225E**.

16 C. Pan, Y. Feng-Jing, Z. Zi-Zhong, H. Bo, W. Li-Bo and Z. Ya-Xun, Enhancement of 2.0 μm fluorescence emission in new $Ho^{3+}/Tm^{3+}/Yb^{3+}$ tri-doped tellurite glasses, *Optoelectron. Lett.*, 2016, **12**(5), 0341, DOI: **10.1007/s11801-016-6145-8**.

17 H. K. Dan, D. C. Zhou, R. F. Wang, Q. Jiao, Z. W. Yang, Z. G. Song, X. Yu and J. B. Qiu, Effect of Mn^{2+} ions on the enhancement red upconversion emission and energy transfer of $Mn^{2+}/Tm^{3+}/Yb^{3+}$ tri-doped transparent glass-ceramics, *Mater. Res. Bull.*, 2016, **73**, 357–361, DOI: **10.1016/j.materresbull.2015.09.019**.

18 L. Z. Xia, Y. Zhang, X. J. Shen and Y. X. Zhou, Broad and flat dual-band NIR luminescence from $Er^{3+}/Tm^{3+}/Ho^{3+}$ tri-doped tellurite glass, *Opt. Lett.*, 2021, **46**(9), 2031–2034, DOI: **10.1364/OL.418971**.

19 N. M. Ty, D. C. Zhou, J. B. Qiu and H. K. Dan, Broadband flat near/mid-infrared emissions of $Tm^{3+}-Ho^{3+}$ co-doped, and $Tm^{3+}-Ho^{3+}-Yb^{3+}$ tri-doped zinc silicate glasses under 808 and 980 nm, *Infrared Phys. Technol.*, 2020, **111**, 103483, DOI: **10.1016/j.infrared.2020.103483**.

20 N. Shasmal, W. J. G. J. Faria, A. S. Stucchi de Camargo and A. C. M. Rodrigues, Enhancement in green and NIR emissions of Er^{3+} by energy transfer from ZnSe nanoparticles in borosilicate glass, *J. Alloys Compd.*, 2021, **863**(15), 158428, DOI: **10.1016/j.jallcom.2020.158428**.

21 A. Roy, A. Dwivedi, H. Mishra, A. K. Rai and S. B. Rai, Generation of color tunable emissions from $Ho^{3+}/Tm^{3+}/Yb^{3+}$ co-doped $YTaO_4$ phosphors through NIR excitation under different conditions (variation of concentration, excitation pump power and the external temperature), *J. Alloys Compd.*, 2021, **865**, 158938, DOI: **10.1016/j.jallcom.2021.158938**.

22 M. Kochanowicz, J. Żmojda, P. Miluski, A. Baranowska, T. Ragin, J. Dorosz, M. Kuwik, W. A. Pisarski, J. Pisarska, M. Leśniak and D. Dorosz, 2 μm emission in gallo-germanate glasses and glass fibers co-doped with Yb^{3+}/Ho^{3+} and $Yb^{3+}/Tm^{3+}/Ho^{3+}$, *J. Lumin.*, 2019, **211**, 341–346, DOI: **10.1016/j.jlumin.2019.03.060**.

23 H. K. Dan, N. D. Trung, D. C. Zhou and J. B. Qiu, Influences of Mn^{2+} ions, and $Mn^{2+}-Yb^{3+}$ dimer on the optical band gaps and bandwidth flatness of near-infrared emissions of Ho^{3+}/Tm^{3+}, $Ho^{3+}/Tm^{3+}/Yb^{3+}$ co-doped calcium aluminosilicate glasses, *J. Non-Cryst. Solids*, 2023, **603**, 122086, DOI: **10.1016/j.jnoncrysol.2022.122086**.

24 H. Masai, T. Nishibe, S. Yamamoto, T. Niizuma, N. Kitamura, T. Akai, T. Ohkubo and M. Yoshida, Low melting oxide glasses prepared at a melt temperature of 500 °C, *Sci. Rep.*, 2021, **11**, 214, DOI: **10.1038/s41598-020-80424-9**.

25 H. K. Dan, N. D. Trung, T. H. Le, N. L. Thai, N. M. Ty, D. C. Zhou and J. B. Qiu, Influence of F^- on the reduction process of Eu^{3+} to Eu^{2+} and optical properties of $Eu^{3+}/Eu^{2+}-Er^{3+}-Yb^{3+}$ co-doped niobate silicate glasses, *J. Non-Cryst. Solids*, 2022, **581**, 121417, DOI: **10.1016/j.jnoncrysol.2022.121417**.

26 H. K. Dan, D. C. Zhou, R. F. Wang, Q. Jiao, Z. W. Yang, Z. G. Song, X. Yu and J. B. Qiu, Effect of Mn^{2+} ions on the enhancement red upconversion emission of $Mn^{2+}/Er^{3+}/Yb^{3+}$ tri-doped in transparent glass-ceramics, *Opt. Laser Technol.*, 2014, **64**, 264–268, DOI: **10.1016/j.optlastec.2014.05.002**.

27 Y. G. Liao, X-ray emission lines & Periodic table for EDS analysis, *Practical electron microscopy and database – An Online Book*, **https://www.globalsino.com/EM**, accessed 15 August, 2023.

28 H. K. Dan, N. D. Trung, N. M. Tam, L. T. Ha, C. V. Ha, D. C. Zhou and J. B. Qiu, Optical band gaps and spectroscopy properties of $Bi^+/Eu^{n+}/Yb^{3+}$ co-doped (m = 0, 2, 3; and n = 2, 3) zinc calcium silicate glasses, *RSC Adv.*, 2023, **13**, 6861–6871, DOI: **10.1039/d2ra07310b**.

29 Y. Tsang, B. Richards, D. Binks, J. Lousteau and A. Jha, A $Yb^{3+}/Tm^{3+}/Ho^{3+}$ triply doped tellurite fiber laser, *Opt. Express*, 2008, **16**(14), 10690–10695, DOI: **10.1364/OE.16.010690**.

30 H. K. Dan, N. M. Ty, D. C. Zhou, J. B. Qiu and A.-L. Phan, Influence of Cr^{3+} on yellowish-green UC emission and energy transfer of $Er^{3+}/Cr^{3+}/Yb^{3+}$ tri-doped zinc silicate glasses, *J. Am. Ceram. Soc.*, 2020, **103**(11), 1–13, DOI: **10.1111/jace.17359**.

31 B. T. Huy, D. H. Kwon, S.-S. Lee, V.-D. Dao, H. B. Truong and Y.-I. Lee, Optical properties of Sr2YF7 material doped with Yb3+, Er3+, and Eu3+ ions for solar cell application, *J.*

Alloys Compd., 2022, **897**, 163189, DOI: **10.1016/j.jallcom.2021.163189**.

32 H. K. Dan, D. C. Zhou, R. F. Wang, Q. Jiao, Z. W. Yang, Z. G. Song, X. Yu and J. B. Qiu, Effect of Mn^{2+} ions on the enhancement upconversion emission and energy transfer of $Mn^{2+}/Tb^{3+}/Yb^{3+}$ tri-doped transparent glass-ceramics, *Mater. Lett.*, 2015, **150**, 76–80, DOI: **10.1016/j.matlet.2015.03.005**.

33 W. Ahmina, M. E. Moudane, M. Zriouil and M. Taibi, Glass-forming region, structure and some properties of potassium manganese phosphate glasses, *Phase Transform.*, 2016, **89**, 1051–1061, DOI: **10.1080/01411594.2016.1144057**.

34 J. de Clermont-Gallerande, D. Taniguchi, M. Colas, P. Thomas and T. Hayakawa, High-temperature investigation of TeO_2–Na_2O–ZnO glasses, *Phys. Status Solidi B*, 2022, **259**, 2200065, DOI: **10.1002/pssb.202200065**.

35 P. Pascuta, G. Borodi, N. Jumate, I. Vida-Simiti, D. Viorel and E. Cule, The structural role of manganese ions in some zinc phosphate glasses and glass ceramics, *J. Alloys Compd.*, 2010, **504**, 479–483, DOI: **10.1016/j.jallcom.2010.05.147**.

36 G. Bai, Y. Guo, Y. Tian, L. Hu and J. Zhang, Light emission at 2 μm from Ho–Tm–Yb doped silicate glasses, *Opt. Mater.*, 2011, **33**(8), 1316–1319, DOI: **10.1016/j.optmat.2011.03.033**.

37 C. Z. Wang, Y. Tian, X. Y. Gao, Q. H. Liu, F. F. Huang, B. P. Li, J. J. Zhang and S. Q. Xu, Mid-infrared fluorescence properties, structure and energy transfer around 2 μm in Tm^{3+}/Ho^{3+} co-doped tellurite glass, *J. Lumin.*, 2018, **194**, 791–796, DOI: **10.1016/j.jlumin.2017.09.052**.

38 G. Y. Zhao, L. Z. Xu, S. H. Meng, C. B. Du, J. S. Hou, Y. F. Liu, Y. Y. Guo, Y. Z. Fang, M. S. Liao, J. Zou and L. L. Hu, Facile preparation of plasmon enhanced near-infrared photoluminescence of Er^{3+}-doped Bi_2O_3-B_2O_3-SiO_2 glass for optical fiber amplifier, *J. Lumin.*, 2019, **206**, 164–168, DOI: **10.1016/j.jlumin.2018.10.026**.

39 Z. Y. Zhao, C. Liu, M. L. Xia, J. Wang, J. J. Han, J. Xie and X. J. Zhao, Effects of Y^{3+}/Er^{3+} ratio on the 2.7 μm emission of Er^{3+} ions in oxyfluoride glass-ceramics, *Opt. Mater.*, 2016, **54**, 89–93, DOI: **10.1016/j.optmat.2016.02.022**.

40 T. G. Mayerhöfer, S. Pahlow and J. Popp, The Bouguer-Beer-Lambert Law: Shining light on the obscure, *ChemPhysChem*, 2020, **21**, 2029–2046, DOI: **10.1002/cphc.202000464**.

41 N. Ilie, A. C. Ionescu, K. C. Huth and M. Moldovan, Light transmission characteristics and cytotoxicity within a dental composite color palette, *Materials*, 2023, **16**, 3773, DOI: **10.3390/ma16103773**.